A Flexible Catheter System for Ultrasound-Guided Magnetic Projectile Delivery

Jakub Sikorski, *Member, IEEE*, Christoff Marthinus Heunis, *Student Member, IEEE*, Rafic Obeid, Venkatasubramanian Kalpathy Venkiteswaran, *Member, IEEE*, and Sarthak Misra, *Senior Member, IEEE*

***Abstract*—Magnetic actuation is a versatile technology, widely applied in medical robotics for noncontact steering of flexible instruments and untethered agents. In this article, we exploit the benefits of this technology by developing a magnetically actuated flexible catheter capable of the controlled ejection and retrieval of an untethered magnetic capsule. The catheter is actuated by the advanced robotics for magnetic manipulation system. The scanning ultrasound is used for 3-D shape reconstruction of the catheter, with a mean error of 0.37 mm. We use a closed-loop position controller to steer the catheter, reporting a mean error of 0.82 mm. We develop a dynamic model of the capsule and use it to predict the trajectory of the projectile. We demonstrate the targeting of the capsule utilizing the null-space of the catheter actuation (mean residual tip displacement of 0.8 mm). Finally, we perform a delivery of a capsule to and retrieval from a target inaccessible for the catheter tip, demonstrating the capability of our instrument to reach challenging locations.**

***Index Terms*—Magnetic Devices, medical robots and systems, motion control, surgical robotics: steerable catheters/needles.**

I. Introduction

In THE last decade, the magnetic actuation has become one of the most promising technologies for noncontact steering of robotic medical devices. The capability of remotely exerting a magnetic wrench at any point within a given workspace has a potential of shifting the design paradigms for steerable medical instruments. By employing magnetic actuation instruments for minimally invasive surgery (MIS) can be made safer, smaller, and more dexterous than the ones currently used in clinical practice [1].

The advantages of magnetic actuation are particularly prominent in the field of flexible surgical instruments. Magnetism has been employed to create steerable catheters which are not burdened with the problems of friction, hysteresis, and backlash inherent to classical tendon-driven actuation [2]. Several studies have demonstrated controlled motion of simple magnetic catheters designed for procedures within the cardiovascular system [3]–[6]. Furthermore, the recent surge of research in this field provided means through which magnetic catheters can enable a whole new group of MIS procedures. Examples include catheters with controllable mechanical properties or functionalized elements, allowing tasks such as grasping, cutting, or tissue coagulation [5], [7]–[9].

Concurrently with the research on flexible catheters, the use of small-scale untethered agents as novel surgical tools has also attracted abundant scientific attention due to the ability of these agents to interact with the human body at submillimeter scale [10]. Magnetic actuation is one of the key technologies enabling noncontact controlled movement of these agents [11]. Specifically, magnetic untethered milli-/micro-robotic agents have been demonstrated to perform various clinically relevant tasks such as targeted drug delivery, grasping, or tissue penetration [12]–[14]. An extensive review of current advances in the field of medical milli-/micro-robotics is presented by Sitti *et al.* [15].

Despite the clinical potential demonstrated by magnetic catheters and untethered milli-/micro-robotic agents in numerous studies, the practical applications of these devices are limited by sets of complementary challenges. Magnetic catheters are burdened with high-bandwidth dynamical behavior due to their continuously bending structure [16]. Control of this behavior is challenging, which limits the reach and precision of instruments integrated into the catheters, usually at their distal end (tip) [6]. This is particularly pronounced when large deflections are required to operate in anatomically complex locations. [4]. Nevertheless, the continuum structure allows the catheters to easily traverse large distances inside the simple, tubular cavities of human body, such as blood vessels or urinary tract, relying on compliance matching for safety [17]. In turn, covering large distances is challenging for untethered milli-/micro-robotic agents. However, once they are successfully delivered close to their final target, they can precisely follow challenging (e.g., tightly curved) trajectories.

Manuscript received April 15, 2021; revised September 1, 2021; accepted October 16, 2021. This work was supported in part by the European Research Council (ERC) under the European Union's Horizon 2020 Research and Innovation programme under Grant 638428 (Project ROBOTAR) and in part by the Netherlands Organization for Scientific Research (NWO) through the Innovational Research Incentives Scheme under Grant VIDI #14855 (Project SAMURAI). This paper was recommended for publication by Associate Editor A. Krupa and Editor A. Menciassi upon evaluation of the reviewers' comments. *(Corresponding author: Jakub Sikorski.)*

Jakub Sikorski, Christoff Marthinus Heunis, Rafic Obeid, and Venkatasubramanian Kalpathy Venkiteswaran are with the Surgical Robotics Laboratory, Department of Biomechanical Engineering, University of Twente, 7522, NB Enschede, The Netherlands (e-mail: j.sikorski@utwente.nl; c.m.heunis@utwente.nl; rafik.obeid@hotmail.com; v.kalpathyvenkiteswaran@utwente.nl).

Sarthak Misra is with the Surgical Robotics Laboratory, Department of Biomechanical Engineering, University of Twente, 7522, NB Enschede, The Netherlands, also with the Department of Biomedical Engineering, University of Groningen, and University Medical Centre Groningen, 9712, CP Groningen, The Netherlands (e-mail: s.misra@utwente.nl).

This article has supplementary material provided by the authors and color versions of one or more figures available at https://doi.org/10.1109/TRO.2021.3123865.

Digital Object Identifier 10.1109/TRO.2021.3123865

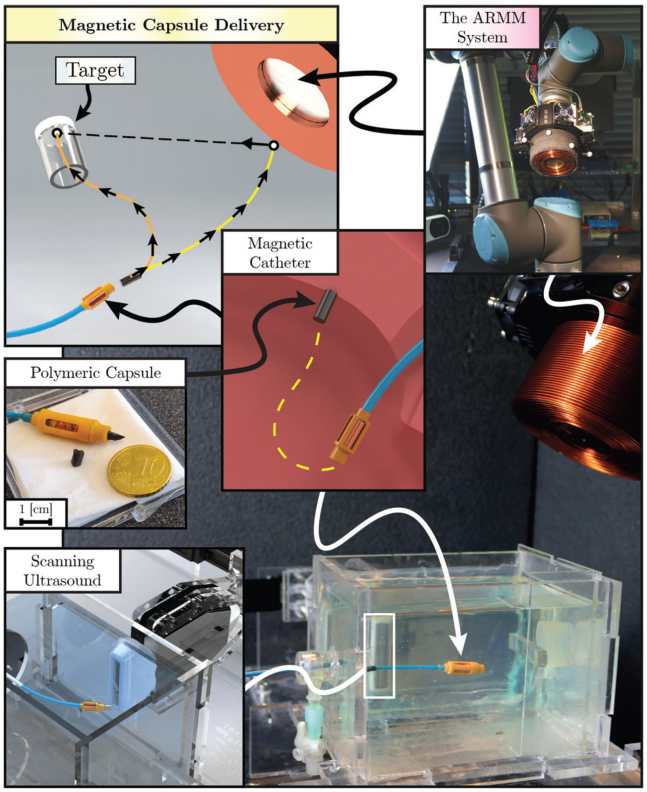

Fig. 1. In this study, we present a magnetic catheter capable of controlled release of untethered capsules fitted in the dock at the catheter tip. The position of that tip is controlled under the guidance of scanning ultrasound. The catheter is actuated using external magnetic field provided by the ARMM system. Upon reaching a desired target, the capsule is ejected by reversing the direction of the current in a miniaturized electromagnet integrated into the catheter tip. We deliver our capsules using an open-loop approach. Upon ejection, the capsule moves as a projectile in the static magnetic field of the ARMM system along a fixed trajectory (yellow line). Using a state-space model of the projectile, we can predict that trajectory. Since our system is overactuated, the reconfiguration of the ARMM system can be used for retargeting the projectile, such that it reaches a desired target (orange line).

The complementary characteristics of catheters and milli-/micro-robotic agents can be exploited to create advanced magnetic surgical instruments. By using design principles associated with both classes of devices within a single system, the inherent advantages of one class can be used to offset the limitations of the other one. A recent study, presenting a mobile, yet tethered magnet as a tool for force control could be considered an early example of this approach [18]. Nevertheless, to the authors' best knowledge, the area remains unexplored in terms of advanced catheter designs capable of autonomous operations in clinically relevant tasks.

In this article, we demonstrate a robotic instrument, which combines a catheter and a milli-robotic agent within a single, magnetically actuated device. Our catheter (Fig. 1) has a miniaturized electromagnetic coil at its tip. This coil can be employed to steer the catheter using external magnetic field provided by the advanced robotics for magnetic manipulation (ARMM) system [19]. Furthermore, since the magnetic field of the miniaturized coil is controllable, we employ the catheter for controlled release and retrieval of an untethered, magnetic, millimeter-scale capsule. The catheter, transporting the capsule at its tip, can be steered into a deeply seated location within the body using the external magnetic field of the ARMM system. Upon arrival within the target workspace, the capsule is ejected from its tip and magnetically steered as an untethered agent. This way, we are capable of accessing locations, which are beyond the reach of the tip of the catheter.

Throughout the procedure, we track our catheter using an ultrasound scanner. We also use this modality to realize closed-loop position control, guiding the catheter tip to the location, where the capsule is to be released. Once ejected, the capsules are considered to behave as projectiles moving in static magnetic field provided by the ARMM system. We demonstrate that, by reconfiguring the ARMM system within the null-space of magnetic actuation, the capsules can often be targeted to reach a given location while keeping the catheter tip steady. We show that this approach readily allows to access targets inaccessible for the catheter itself. Additionally, we derive a dynamical model describing the projectile motion. We show that this model can be used to predict capsule trajectory and analyze the set of reachable targets for a given configuration of the catheter. Our platform can in the future serve for clinically relevant tasks, such as targeted drug delivery or biopsies, performed in challenging locations.

The rest of this article is structured as follows. Section II introduces the design of our catheter for the delivery of untethered capsules and the experimental setup used to test it. In Section III, the ultrasound-based shape reconstruction technique used in this article is presented and validated. Section IV describes the closed-loop position controller of the catheter tip and its experimental validation. Section V concerns the motion of the ejected capsule, introducing its dynamic model and demonstrating how to use this model to compute a set of reachable targets for a particular catheter configuration. Section VI contains the experiments on various aspects of catheter-based capsule delivery. In Section VII, we provide a general discussion of all our findings. Finally, Section VIII concludes this article.

II. Magnetic Catheter for Capsule Delivery: System Composition

The system presented in this article exploits the principles of magnetic actuation. This technique utilizes external magnetic field ($\mathbf{B}(\mathbf{p}) \in \mathbb{R}^3$) to generate magnetic wrenches ($\mathbf{w}_\mu \in \mathbb{R}^6$) acting on a magnetic object located at a point ($\mathbf{p} \in \mathbb{R}^3$). If the magnetic object is represented by its dipole moment ($\boldsymbol{\mu} \in \mathbb{R}^3$), the resulting magnetic wrench on the object can be described as follows:

$$\mathbf{w}_\mu = \begin{bmatrix} \mathbf{f}_\mu \\ \boldsymbol{\tau}_\mu \end{bmatrix} = \begin{bmatrix} \nabla \left(\boldsymbol{\mu}^T \mathbf{B}(\mathbf{p}) \right) \\ S\left(\boldsymbol{\mu}\right) \mathbf{B}(\mathbf{p}) \end{bmatrix} \tag{1}$$

where $\boldsymbol{\tau}_\mu \in \mathbb{R}^3$ is the magnetic torque due to the magnetic field, $\mathbf{f}_\mu \in \mathbb{R}^3$ is the magnetic force dependent on its spatial gradient ($\nabla \mathbf{B} \in \mathbb{R}^{3\times3}$), and, for any vector, the operator S represents its skew-symmetric form.

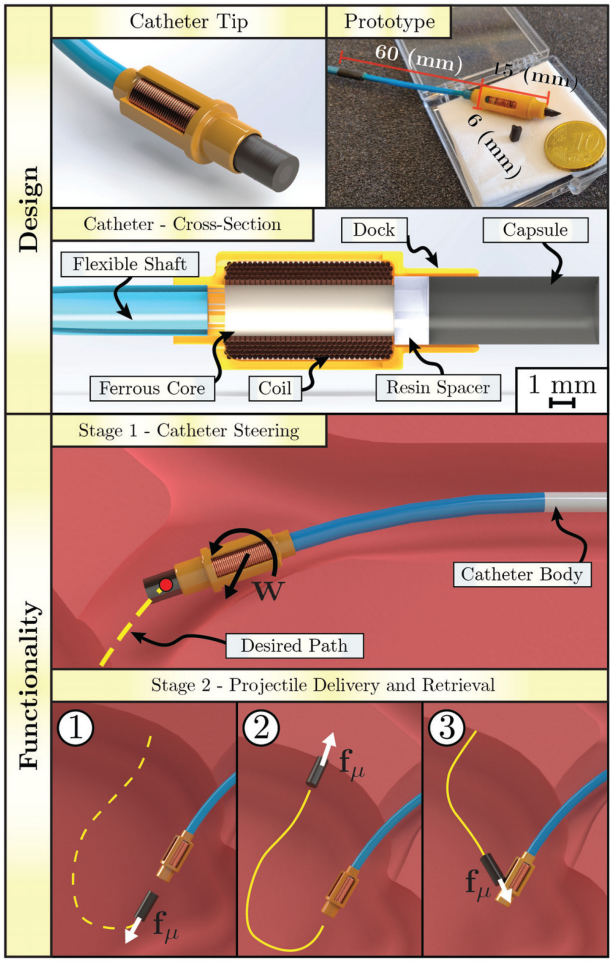

Fig. 2. **Design:** A magnetic catheter can be used to deliver and retrieve untethered capsules to challenging locations. **Functionality:** Initially, the capsule is attracted to the electromagnetic coil at the tip of the catheter. The catheter in such a configuration is steered to the target site using magnetic wrenches ($\mathbf{w} \in \mathbb{R}^6$) due to external field. ① Once close to the target, the capsule is released by changing the direction of the current in the miniaturized coil. ② The ejected capsule moves (yellow) as a projectile under the influence of magnetic force ($\mathbf{f}_\mu \in \mathbb{R}^3$) due to external field. The capsule can be used as a platform for tasks such as biopsy or targeted drug delivery. ③ After the completion of such a task, the capsule is retrieved from the target site by steering it to the vicinity of the catheter tip.

A. *Catheter Design and Functionality*

Our catheter is designed exploiting the magnetic interaction (1) between two components: a miniaturized electromagnet and a polymeric capsule (Fig. 2, Top). The capsule is made of a soft composite with a hard magnetic phase, whose net magnetization is represented by a dipole moment ($\boldsymbol{\mu}_p \in \mathbb{R}^3$). It is fitted inside a rigid dock, located at the tip of the catheter. The miniaturized coil is also located at the tip, proximally to the capsule dock. The coil is magnetized by the current ($I_c \in \mathbb{R}$), which we represent by a magnetic dipole moment ($\boldsymbol{\mu}_c \in \mathbb{R}^3$).

The three-way interaction between the capsule, the electromagnet, and the external magnetic field can be used in a number of ways. The miniaturized coil can be used to attract or repel a capsule. The external magnetic field can deflect the catheter or propel a detached capsule. This broad set of interactions can be used sequentially to realize a procedure, where the soft capsule is delivered to a target site, detached, guided to its final destination, and then again retrieved by the catheter (Fig. 2, Stages 1 and 2). Since the capsule is an untethered agent, it is able to reach locations inaccessible to the tip of the catheter.

Our procedure can be divided into two stages. In Stage 1, the magnetic attraction between the two dipoles is used to stabilize the position of the capsule. This permits the navigation of the catheter to the target site. Since the coil and the capsule are effectively a part of the same rigid body, we use the interaction of their combined dipole moment ($\boldsymbol{\mu}$) with a source of external magnetic field to control the catheter tip position using magnetic wrenches ($\mathbf{w}$).

Upon reaching the target area, Stage 2 of our procedure can take place. Once the tip is close to the target, we eject the capsule from the dock by reversing the current (I_c), which creates a strong repulsive force. Upon release, the capsule moves as an untethered projectile. It can be guided toward its final target using the source external magnetic field.

The untethered capsule is assumed to be functionalized for a specific task, such as drug delivery. After the completion of that task, the capsule can be retrieved by the catheter. For that purpose, the capsule must be brought to the vicinity of the miniaturized electromagnet by external forces. Once the capsule gets attracted to the catheter tip, the entire system can be retracted from the workspace.

B. *Prototype Fabrication*

Our catheter is validated in a proof-of-concept study involving a functional prototype. The prototype (Fig. 2) comprises an electromagnetic tip mounted onto the flexible shaft extruded from Pebax 6333 thermoactive polymer (length 60 mm, ø 2 mm). The outer shell of the end-effector is fabricated from a photoactive resin using stereolitographic 3-D printing (Prusa SL1, Prusa Research, Prague, Czech Republic). In the proximal compartment of the end effector, we locate a custom-made copper-wire electromagnetic coil with stainless steel core (coil ø 6 mm, core ø 3 mm, wire ø 0.25 mm, length 10 mm, and resistance 1.1 Ω) powered by insulated leads, which are fixed inside the flexible shaft. The coil is powered by a current of 0.75 A supplied by an iPOS4808 BX-CAT current controller (Technosoft Motion, Neuchatel, Switzerland).

The soft magnetic capsules used in the proof-of-concept study are fabricated of a composite comprising Ecoflex™ 00-10 (Smooth-On Inc., Macungie, PA, USA) silicone rubber mixed with praseodymium-iron-boron (PrFeB) hard magnetic particles (MQFP-16-7-11277, Magnequench GmbH, Germany). The rubber and the particles are mixed in 1:1 ratio by mass. The composite is cured, forming a large cylindrical block (ø 20 mm, height 100 mm), which is subsequently magnetized under the field of 2 T. Finally, the block is cut into individual capsules (length 6 mm ø 4 mm).

C. *Experimental Setup*

We test our catheter experimentally in a dedicated test-bed shown in Fig. 3. The catheter is inserted into a Poly methyl

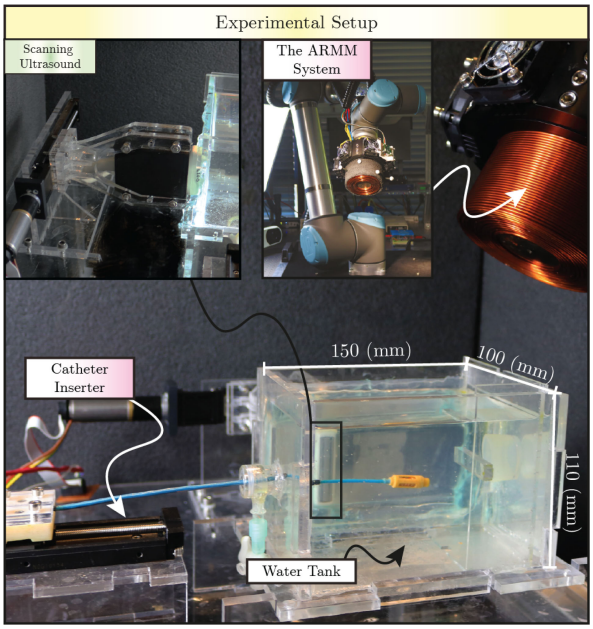

Fig. 3. Test-bed used for experimental studies involving our magnetic catheter. The ARMM system is used to control the catheter in a water-filled tank. The catheter is inserted into the tank using an LX15 linear actuator (Misumi Europa GmbH, Schwalbach am Taunus, Germany). During the experiments, the catheter is tracked using the scanning ultrasound technique through an ultrasound-transparent wall made out of silicon rubber.

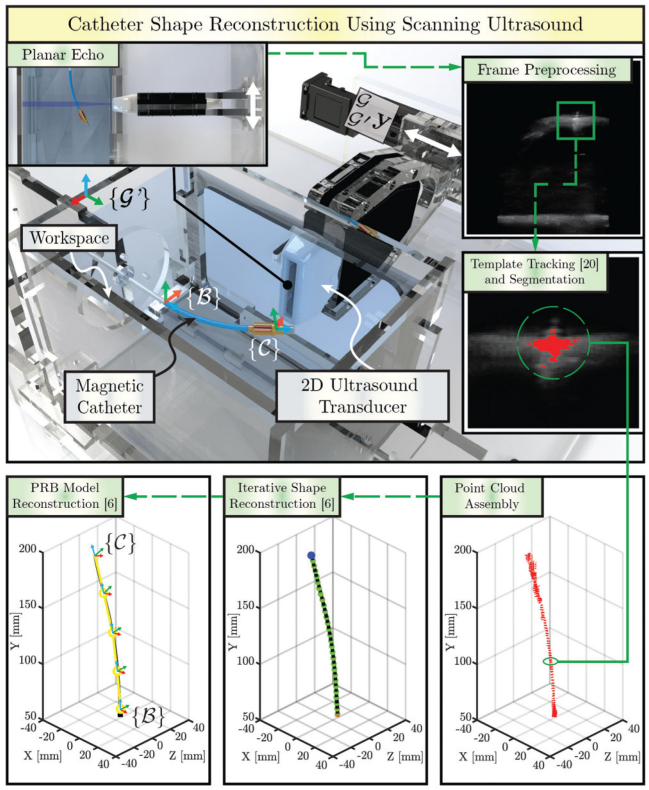

Fig. 4. PRB configuration of the catheter is reconstructed by using volumetric ultrasound scan technique. A 14-MHz L14-5/38 2-D ultrasound transducer of the Ultrasonix SonixTouchQ+ system (BK Medical, Peabody, MA, USA) is located in the workspace and registered with respect to its frame of reference ($\{\mathcal{G}'\}$). The transducer is periodically swept along ($^{\mathcal{G}}_{\mathcal{G}'}\widehat{\mathbf{y}} \in \mathbb{R}^3$). A stack of position-ordered two-dimensional ultrasound frames is collected during a single sweep. The silhouette of the catheter, spanning between the frames at its base ($\{\mathcal{B}\}$) and tip ($\{\mathcal{C}\}$), is extracted from the stack iteratively by a template-based tracker similar to [20]. The PRB model is then reconstructed from the resulting point-cloud by using the technique presented in our previous work [6].

metacrylate (PMMA) tank filled with water, using LX15 linear actuator (Misumi Europa GmbH, Schwalbach am Taunus, Germany), position-controlled using iPOS4808 BX-CAT drives (Technosoft Motion). The ultrasound scanner is mounted at the side of the tank, imaging the water-filled volume through a silicon membrane.

As mentioned earlier, the steering of our catheter requires a source of external magnetic field ($\mathbf{B}(\mathbf{p})$). For the purpose of this study, we integrate our catheter within the ARMM system. This system uses a mobile coil fixed on a UR10 robotic arm (Universal Robots, Odense, Denmark), being capable of generating $\mathbf{B}(\mathbf{p})$ in workspaces spanning the entire human body. A detailed description of the system and the rationale behind its design are presented in our prior work [19].

III. Catheter Shape Reconstruction Using Scanning Ultrasound

As our magnetic catheter is designed to operate within the confines of the human body, a clinically relevant feedback modality must be available, providing information about the configuration and location of the catheter for the purpose of closed-loop control. For that purpose, we employ ultrasound. During all stages of operation, we acquire volume scans of the catheter within its environment using a mobile 2-D ultrasound probe. Subsequently, the scans are processed to segment the silhouette of the catheter and retrieve its mechanical configuration.

A. Ultrasound Scanner: System Composition

We realize this method, using an ultrasound scanner system (Fig. 4), built specifically for the study. The scanner comprises a 14-MHz L14-5/38 2-D ultrasound transducer (Ultrasonix SonixTouchQ+, BK Medical, Peabody, MA, USA) on a motorized linear stage. During the catheter navigation, the scanner sweeps the transducer periodically between two position limits, producing two-dimensional B-mode images (660×616 pixels each) at 36 Hz (Fig. 4). A stack of these images, along with their locations expressed in workspace frame of reference ($\{\mathcal{G}'\}$), is recorded for each sweep of the scanner.

The silhouette of the catheter is located on each B-mode image using a template tracker described by Kaya *et al.* [20]. This tracker has been used in conjunction with a point-cloud assembly technique devised specifically for this study. The pixels comprising the silhouette are segmented based on a constant threshold value. Pixels from all processed ultrasound images are assembled into a point-cloud using the information about the position of each image within the stack.

The point-cloud is processed by an iterative algorithm, which has already been presented in our previous work [6]. This

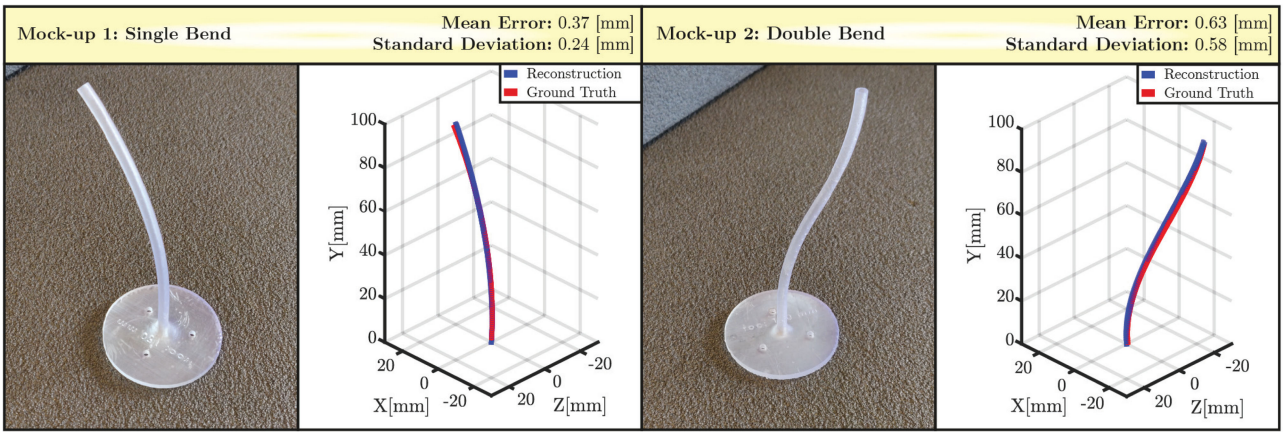

Fig. 5. Accuracy of the catheter tracking using scanning ultrasound technique is established using two mock-ups with predefined shapes as a ground truth. The mock-ups are 3-D printed and fixed in a known pose within the experimental test-bed. The ultrasound scanner is used to collect five independent stacks of B-mode images corresponding to each mock-up. Each stack is processed using our shape reconstruction algorithm to recover a polynomial model. The same polynomial model is fitted onto a set of points along the centerline of each mock-up, generating ground truth. The error metrics are generated by comparing the positions of 100 points at corresponding lengths along the continuous shape. The errors between the shapes reconstructed from individual stacks are negligible (below 0.1 mm).

algorithm provides a sixth-order polynomial representing the shape of the catheter as a continuous function. This polynomial function is subsequently processed to fit a kinematic model describing the configuration of the catheter in global reference frame. The sixth order has been deemed optimal based on the validation presented in [6].

B. Validation of Ultrasound Shape Reconstruction

We quantify the accuracy of our shape reconstruction method using two mock-ups with known shapes as a ground truth (Fig. 5). The mock-ups are designed using SolidWorks 2018 CAD (Dassault Systèmes, Vélizy-Villacoublay, France) and printed using Form2 SLA 3D printer (Formlabs Inc., Somerville, MA, USA). Subsequently, they are fixed within the test-bed, with their poses registered with respect to the frame $\{\mathcal{G}\}$. The ultrasound scanner is used to acquire five independent stacks of images representing each mock-up.

Each image stack is processed independently by our shape reconstruction algorithm (Fig. 4) to obtain a polynomial representation. Subsequently, the CAD models are converted into a set of points along the centerline of each mock-up. These points are used to fit the ground truth polynomials. The ground truth is compared with the reconstruction by using the respective polynomials to generate sets of 100 3-D points at corresponding positions along the shape.

The results (Fig. 5) show good correspondence of the reconstructed shapes with the ground truth with the mean errors of 0.37 and 0.63 mm. We additionally quantify the standard deviations of the errors, which are 0.24 and 0.58 mm for mock-ups 1 and 2, respectively. The discrepancies between the individual scanning stacks are negligible (below 0.1 mm). This allows us to conclude that the scanning ultrasound has sufficient precision as a tracking method for our magnetic catheter.

IV. Position Control of a Catheter Using a Mobile Electromagnet

In this section, we propose a method for autonomous steering of the tip of a magnetic catheter with a single mobile electromagnet. We model the system, considering four principal coordinate reference frames. The frames are shown in Fig. 6. The global reference frame $(\{\mathcal{G}\})$ is located at the base of the robotic arm. The generalized coordinates of the UR10 joints $(\mathbf{q}_m \in \mathbb{S}^6)$ define the pose of the end-effector frame $(\{\mathcal{T}\})$ located on the distal face of the electromagnet. The mathematical description of the catheter uses two frames: $\{\mathcal{B}\}$ at its base and $\{\mathcal{C}\}$ at its tip.

The linear transformation between any two frames $(\{\mathcal{J}\})$ and $(\{\mathcal{K}\})$ is represented by homogeneous transformation matrices $({}^{\mathcal{J}}_{\mathcal{K}}\mathbf{H} \in \mathrm{SE}(3))$ as follows:

$$ {}^{\mathcal{J}}_{\mathcal{K}}\mathbf{H} = \begin{bmatrix} {}^{\mathcal{J}}_{\mathcal{K}}\mathbf{R} & {}^{\mathcal{J}}_{\mathcal{K}}\mathbf{p} \\ \mathbf{0}_{1\times 3} & 1 \end{bmatrix} \tag{2} $$

where

$$ {}^{\mathcal{J}}_{\mathcal{K}}\mathbf{R} = \begin{bmatrix} {}^{\mathcal{J}}_{\mathcal{K}}\hat{\mathbf{x}} & {}^{\mathcal{J}}_{\mathcal{K}}\hat{\mathbf{y}} & {}^{\mathcal{J}}_{\mathcal{K}}\hat{\mathbf{z}} \end{bmatrix} \in \mathrm{SO}(3), \tag{3} $$

$$ {}^{\mathcal{J}}_{\mathcal{K}}\mathbf{p} = \begin{bmatrix} {}^{\mathcal{J}}_{\mathcal{K}}x & {}^{\mathcal{J}}_{\mathcal{K}}y & {}^{\mathcal{J}}_{\mathcal{K}}z \end{bmatrix}^T \in \mathbb{R}^3. \tag{4} $$

The matrices associated with the end-effector frame $(\{\mathcal{T}\})$ are calculated from instantaneous generalized coordinates $(\mathbf{q}_m)$ of the ARMM system [21]. The pose of the catheter is retrieved using the scanning ultrasound technique.

A. Tip Position Controller

In our steering strategy, the forward motion of the catheter is provided by an automated inserter, capable of applying arbitrary displacements $(\lambda \in \mathbb{R})$ along the neutral axis of the catheter $(\widehat{\boldsymbol{\lambda}} \in \mathbb{R}^3)$. The deflection of the flexible body of the catheter away from that axis is achieved by using the magnetic field

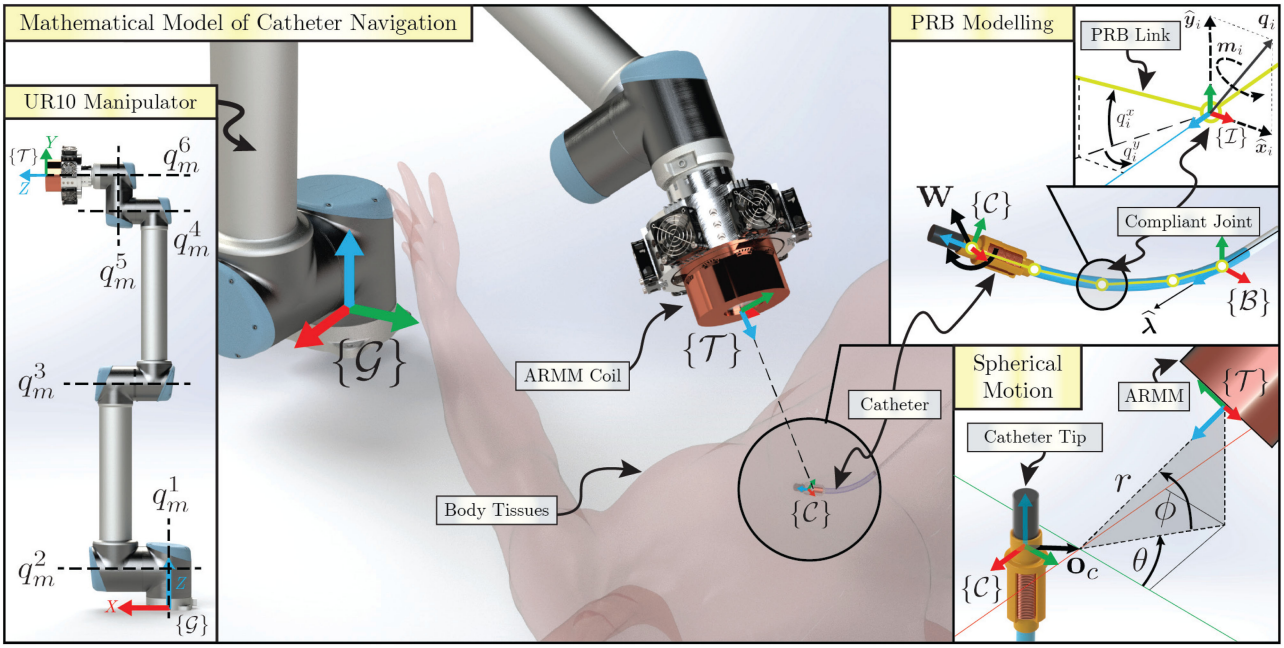

Fig. 6. We demonstrate autonomous operation of our magnetic catheter using the ARMM system as the actuation framework. This system employs a 6-DoF UR10 manipulator (Universal Robots, Odense, Denmark) to position an electromagnetic coil within a large workspace. The magnetic field generated by the ARMM coil interacts with the magnetic element at the tip of the catheter, generating wrenches ($\mathbf{w} \in \mathbb{R}^6$). In order to describe the effect of $\mathbf{w}$ on the shape of the catheter, we use the PRB model, expressed in catheter base frame ($\{\mathcal{B}\}$). This model represents the continuously bending catheter by a series of rigid links connected by compliant joints. Each joint (i) is parametrized by two angle variables ($q_i^x, q_i^y \in \mathbb{S}$), based on the internal bending moment ($\mathbf{m}_i \in \mathbb{R}^3$) at the joint due to external load, including $\mathbf{w}$. The total deflection of all PRB joints determines the pose of the tip frame($\{\mathcal{C}\}$). The actuation model is simplified by imposing a spherical motion model. The UR10 joint variables ($\mathbf{q}_m \in \mathbb{S}^6$) are controlled in such a way that the Z-axis of the ARMM tool frame ($\{\mathcal{T}\}$) always points toward catheter tip ($\{\mathcal{C}\}$), and the offset ($\mathbf{d}_c \in \mathbb{R}^3$) is minimized. The resulting position of the ARMM coil can be parametrized in spherical coordinates ($\mathbf{s} = \begin{bmatrix} r & \theta & \phi \end{bmatrix} \in \mathbb{R}^+ \times \mathbb{S}^2$). By finding the relation between $\mathbf{s}$ and $\mathbf{w}$, the catheter can be remotely navigated in global reference frame ($\{\mathcal{G}\}$) using inverse model control.

($\mathbf{B}({}^{\mathcal{G}}_{\mathcal{C}}\mathbf{p})$) and its gradient ($\nabla\mathbf{B}$) generated by the ARMM system. At any instance of time, the field/gradient depends on the configuration of the electromagnetic coil (${}^{\mathcal{G}}_{\mathcal{T}}\mathbf{H}$) and the current ($I \in \mathbb{R}$) running through it. By controlling these variables, wrenches ($\mathbf{w}_\mu$) can be applied to the effective dipole ($\boldsymbol{\mu}$), which is located at ${}^{\mathcal{G}}_{\mathcal{C}}\mathbf{p}$. We assume this dipole to be constant and invariant to the external magnetic field/gradient.

We model the catheter deflection due to $\mathbf{w}_\mu$ using a quasi-static pseudo-rigid body (PRB) model presented in detail in our previous work [6]. The continuously bending body of the catheter is divided into discrete, pseudo-rigid links, while its stiffness is represented by torsional elements within 2-DoF joints connecting the links. By assuming very slow motion of the catheter, we can neglect its transient dynamics [4]. Thus, analytic relation between the magnetic wrench rate ($\dot{\mathbf{w}}$) and catheter tip velocity becomes

$$\mathbf{J}_a \dot{\mathbf{w}}_\mu = \dot{\mathbf{p}} \tag{5}$$

where $\mathbf{J}_a$ is the catheter actuation Jacobian derived as in [6].

Having independent control over the elements of wrench ($\mathbf{w}_\mu$) would allow us for direct application of (5) in an inverse model controller. However, the ARMM system relies on controlled motion of the coil to generate the desired $\mathbf{B}(\mathbf{p})$. Therefore, the behavior of the ARMM system has to be explicitly taken into account while designing the controller for our catheter. We divide the controller into two cascades, making the inner loop responsible for low-level motion of the UR10 described by a set of parameters. The outer loop will control these parameters to steer the tip position (${}^{\mathcal{G}}_{\mathcal{C}}\mathbf{p}$) along a trajectory. The entire control strategy is summarized in Fig. 7.

At any given configuration, the effect of UR10 joint angles ($\mathbf{q}_m$) and current (I) on the magnetic wrench ($\mathbf{w}$) can be described by a magnetic field model. In our work, we use a multipole expansion approach similar to [22]. The resulting analytic forward model accurately describes magnetic fields and gradients around a coil located at any point in space.

The use of a complete multipole representation for catheter control using a mobile electromagnet is impractical, as it necessitates the use of a highly nonlinear differential formulation. If used in an unconstrained inverse map, this formulation generates fast and unpredictable motion of the magnet for a given field reference trajectory, as observed empirically. As a result, it proves unsafe without collision avoidance algorithms in place. We remedy that by using a set of spherical coordinates to define the position of the coil with respect to the catheter tip. This approach implicitly constrains the motion of the electromagnet. As a result, the behavior of the system improves significantly. Additionally, the motion along the spherical coordinates allows us to intuitively impose constraints on the system by using weighted least-squares approach.

We introduce our approach by assuming that the dipole frame ($\{\mathcal{C}\}$) is always located on axis (${}^{\mathcal{G}}_{\mathcal{T}}\hat{\mathbf{z}}$). Thus, the position of the

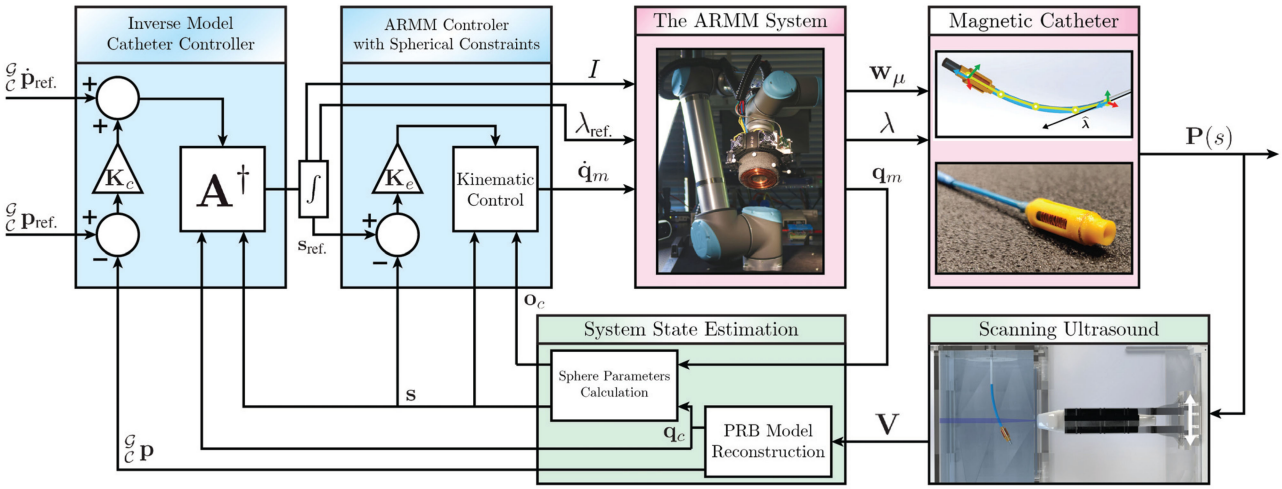

Fig. 7. Control system (blue) proposed in this work is used to track the reference position of the magnetic catheter ($^{\mathcal{G}}_{\mathcal{C}}\mathbf{p}_{\text{ref.}} \in \mathbb{R}^3$). The catheter shape ($\mathbf{P}(s)$, defined as in [6]) is manipulated using the ARMM system by exerting magnetic wrench ($\mathbf{w}_\mu \in \mathbb{R}^6$) at the tip of the catheter and the displacement ($\lambda \in \mathbb{R}$) at its base. The behavior of the ARMM system is driven by specifying the robot joint velocity ($\dot{\mathbf{q}}_m \in \mathbb{R}^7$), reference inserter position ($\dot{\lambda}_{\text{ref.}} \in \mathbb{R}$), and coil current ($I \in \mathbb{R}$). These values are computed in a two-stage control approach. The inner controller enforces spherical motion (Fig. 6) with parameters ($\mathbf{s}_{\text{ref.}} \in \mathbb{R}^+ \times \mathbb{S}^2$). These parameters are calculated by the inverse model controller, which uses the linearized, reduced-order inverse model of the system ($\mathbf{A}^\dagger \in \mathbb{R}^{5\times3}$) to minimize the error between $^{\mathcal{G}}_{\mathcal{C}}\mathbf{p}_{\text{ref.}}$ and the actual position estimate ($^{\mathcal{G}}_{\mathcal{C}}\mathbf{p} \in \mathbb{R}^3$). We provide the feedback to both control stages by tracking the shape of the catheter using linear scanning ultrasound technique. This technique generates a point cloud ($\mathbf{V}$), processed to retrieve the estimates of the PRB configuration of the catheter ($\mathbf{q}_c \in \mathbb{R}^8$). For the purpose of spherical motion control, the actual sphere parameters ($\mathbf{s} \in \mathbb{R}^+ \times \mathbb{S}^2$) and the offset ($\mathbf{o}_c \in \mathbb{R}^3$) between the center of the sphere and the catheter tip are calculated using the information about ARMM and catheter configuration. The gain matrices ($\mathbf{K}_c,\ \mathbf{K}_e \in \mathbb{R}^{3\times3}$) are used to tune the performance of both control stages.

coil can be parametrized by spherical coordinates

$$\mathbf{s} = \begin{bmatrix} r & \theta & \phi \end{bmatrix} \in \mathbb{R}^+ \times \mathbb{S}^2 \tag{6}$$

as shown in Fig. 6. If ($r \in \mathbb{R}^+$) denotes the distance from the face of the coil, the magnetic field and its gradient along that axis expressed in frame ($\{\mathcal{T}\}$) can be computed as follows:

$$\mathbf{B} = I \begin{bmatrix} 0 & 0 & 1 \end{bmatrix}^T b(r, I) \tag{7}$$

$$\nabla\mathbf{B} = \text{diag}\left(\begin{bmatrix} -0.5 & -0.5 & 1 \end{bmatrix}\right) I \frac{\partial b}{\partial r} \tag{8}$$

where ($b(r, I) : \mathbb{R}^+ \times \mathbb{R}^+ \mapsto \mathbb{R}$) is the field model described in detail in the Appendix.

Subsequently, combining (1) and (7), the magnetic wrench ($\mathbf{w}_\mu$) can be expressed in frame ($\{\mathcal{C}\}$) as a function of control parameters ($\mathbf{s}, I$) as follows:

$$\mathbf{w}_\mu(\mathbf{s}, I) = I\mu \begin{bmatrix} -\frac{3}{2}\sin\theta\sin\phi\cos\phi & 0 \\ \frac{3}{2}\cos\theta\sin\phi\cos\phi & 0 \\ \sin^2\phi - \frac{1}{2}\cos^2\phi & 0 \\ 0 & -\cos\theta\cos\phi \\ 0 & -\sin\theta\cos\phi \\ 0 & 0 \end{bmatrix} \begin{bmatrix} \frac{\partial b}{\partial r} \\ b(r) \end{bmatrix}. \tag{9}$$

We initialize the system such that the tip of the catheter is located in the close vicinity of the long axis of the coil ($^{\mathcal{C}}_{\mathcal{T}}\hat{\mathbf{z}}$). Hence, we assume that (7) holds. The UR10 provides direct control over its joint velocities ($\dot{\mathbf{q}}_m$). Hence, we enforce the spherical motion with the inverse Jacobian controller

$$\dot{\mathbf{q}}_m = \mathbf{J}_t^{-1} \left(\begin{bmatrix} \mathbf{K}_o\, {}^{\mathcal{T}}_{\mathcal{C}}\mathbf{R}\, \mathbf{d}_c \\ \mathbf{0}_{3\times1} \end{bmatrix} + \mathbf{K}_e \mathbf{J}_e \mathbf{e}_s \right) \tag{10}$$

where $\mathbf{J}_t \in \mathbb{R}^{6\times6}$ is the UR10 end-effector Jacobian, ($\mathbf{d}_c \in \mathbb{R}^3$) is the offset of the dipole center from the coil axis ($^{\mathcal{C}}_{\mathcal{T}}\hat{\mathbf{z}}$), and $\mathbf{K}_0, \mathbf{K}_e \in \mathbb{R}^{3\times3}$ are the positive-definite gain matrices. The matrix ($\mathbf{J}_e \in \mathbb{R}^{6\times3}$) which is defined as follows:

$$\mathbf{J}_e = \begin{bmatrix} 0 & 0 & -1 & 0 & 0 & 0 \\ r\cos\phi & 0 & 0 & 0 & -\cos\phi & -\sin\phi \\ 0 & r & 0 & -1 & 0 & 0 \end{bmatrix}^T \tag{11}$$

maps the spherical motion to velocity of the origin of frame ($\{\mathcal{T}\}$). The controller minimizes both the offset ($\mathbf{d}_c$) as well as the error ($\mathbf{e}_s = \mathbf{s}_{\text{ref.}} - \mathbf{s}$) between the reference and actual positions expressed in spherical coordinates.

The outer loop of the catheter controller provides reference values for the spherical parameters, the current of the ARMM coil, and the position of the catheter inserter. We define a spherical actuation Jacobian ($\mathbf{J}_s$) $\in \mathbb{R}^{4\times6}$

$$\mathbf{J}_s = \begin{bmatrix} \frac{\partial \mathbf{w}}{\partial \mathbf{s}}^T & \frac{\partial \mathbf{w}}{\partial I}^T \end{bmatrix}^T. \tag{12}$$

This Jacobian is used along with the PRB model (5) to derive an equation describing the effect of all control inputs on the

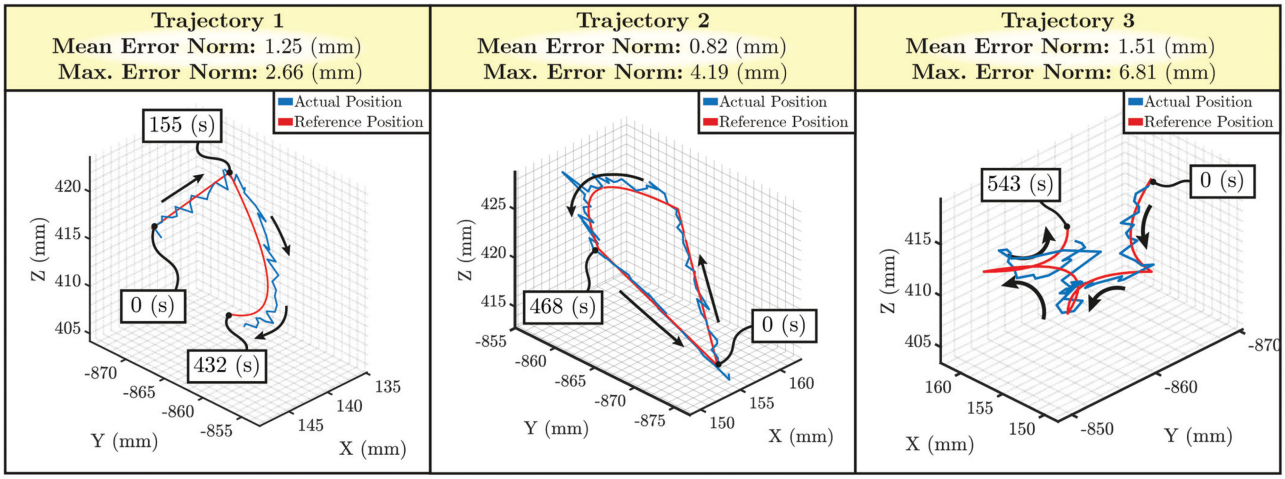

Fig. 8. Closed-loop position controller is tested in an experiment involving steering of the magnetic catheter across three representative trajectories. The 3-D plots present the actual and reference catheter tip position in Cartesian coordinates (X, Y, Z) of global reference frame $(\{\mathcal{G}\})$. (Please refer to the video supplementary material for the demonstration of this experiment.)

catheter tip velocity

$$\mathbf{J}_a \mathbf{J}_s \begin{bmatrix} \dot{\mathbf{s}} \\ \dot{I} \end{bmatrix} + \widehat{\boldsymbol{\lambda}} \dot{\lambda} = \mathbf{A} \begin{bmatrix} \dot{\mathbf{s}} \\ \dot{I} \\ \dot{\lambda} \end{bmatrix} = \mathbf{A}\dot{\boldsymbol{\sigma}} = {}^{\mathcal{G}}_{\mathcal{C}}\dot{\mathbf{p}}. \tag{13}$$

An analytic derivation of $\mathbf{J}_s$ is presented in the Appendix.

Inverting the actuation matrix $(\mathbf{A} \in \mathbf{R}^{3\times5})$ allows us to compute the rate of reference control parameters $(\boldsymbol{\sigma}_{\text{ref.}} \in \mathbb{R}^3 \times \mathbb{S}^2)$ which minimizes the catheter position error

$$\dot{\boldsymbol{\sigma}}_{\text{ref.}} = \mathbf{A}^{\dagger} \left({}^{\mathcal{G}}_{\mathcal{C}}\dot{\mathbf{p}}_{\text{ref.}} + \mathbf{K}_c \mathbf{e}_c \right) \tag{14}$$

where † denotes weighted-damped pseudo-inverse [23], $\mathbf{K}_c \in \mathbb{R}^{3\times3}$ is a positive-definite gain matrix, and $\mathbf{e}_c \in \mathbb{R}^3$ is the trajectory error which is defined as follows:

$$\mathbf{e}_c = {}^{\mathcal{G}}_{\mathcal{C}}\mathbf{p}_{\text{ref.}} - {}^{\mathcal{G}}_{\mathcal{C}}\mathbf{p}. \tag{15}$$

The heuristically established weights in the weighted-damped pseudo-inverse improve the behavior of the resulting solution. In our case, they are predominantly used to limit the displacement rates along r to avoid the collisions of the mobile coil. Additionally, this technique inherently allows imposing limits on control variables, avoiding collisions with a predefined workspace.

B. Position Control: Experimental Results

The tracking and control framework presented in previous sections is implemented in C++ on Linux Ubuntu 16.04 workstation (Kernel 4.4, Intel Xeon E5 CPU, NVidia Quadro K4200 GPU and 32-GB RAM). The inner spherical motion controller (Fig. 7) is timed at 125 Hz, which is the internal rate used by the UR10. The rate of the inverse model controller (14) is limited by the speed of the ultrasound scanner. The system requires approximately 7 s for a single scan.

The inverse-model position controller is tested experimentally in a study involving steering the magnetic catheter through a series of trajectories. Before each trajectory, a volumetric ultrasound scan is taken to align the ARMM system in a predefined position in spherical coordinates $(\mathbf{s})$. The trajectories are defined using point-to-point parabolic segments. The results of the study are shown in Fig. 8. The minimum reported mean error is 0.82 mm for Trajectory 2, whereas Trajectory 1 was executed with the smallest maximum error norm of 2.66 mm. (Please refer to the video supplementary material for the demonstration of this experiment.)

V. Dynamic Modeling of a Magnetic Projectile

Once the catheter reaches the desired region, the magnetic capsule can be deployed and guided to its final target. The catheter releases the capsule when the current in the coil located at its tip is reversed (Fig. 2). The ejected capsule can be subsequently guided to a target site under the influence of the magnetic wrench $(\mathbf{w}^p_{\mu} \in \mathbb{R}^6)$. In this work, we consider an open-loop guidance strategy, in which the capsule is delivered as a projectile following a trajectory determined by the configuration of the ARMM system.

A. Projectile Modeling

The motion of such a projectile can be represented by using a dynamical state-space model. The instantaneous pose of the capsule is represented by a reference frame $(\{\mathcal{P}\})$, which is defined by an instantaneous position vector $({}^{\mathcal{G}}_{\mathcal{P}}\mathbf{p} \in \mathbb{R}^3)$ and orientation quaternion $({}^{\mathcal{G}}_{\mathcal{P}}\mathbf{o} = \begin{bmatrix} o_c & \mathbf{o}_v \end{bmatrix} \in \mathbb{H})$. We assume the capsule to be moving in an external magnetic field $(\mathbf{B}_p({}^{\mathcal{G}}_{\mathcal{P}}\boldsymbol{\sigma}, \mathbf{p}))$, which is composed of superposed fields generated by the magnet of the ARMM system, represented by the multipole expansion model, and the electromagnet at the catheter tip, represented by point dipole with a dipole moment $(\boldsymbol{\mu}_c)$. The trajectory of the capsule is given by the state vector

$$\mathbf{P} = \begin{bmatrix} {}^{\mathcal{G}}_{\mathcal{P}}\mathbf{p}^T & {}^{\mathcal{G}}_{\mathcal{P}}\mathbf{v}^T & {}^{\mathcal{G}}_{\mathcal{P}}\mathbf{o}^T & {}^{\mathcal{P}}_{\mathcal{P}}\boldsymbol{\omega}^T \end{bmatrix}^T \in \mathbb{R}^9 \times \mathbb{H}. \tag{16}$$

TABLE I
IDENTIFICATION OF THE CAPSULE MODEL PARAMETERS

Parameter	Variable	Value
Capsule Mass (mg)	m_p	63.5
Capsule Dipole Moment (Am^2)	$\|\boldsymbol{\mu}_p\|$	$4.3{\cdot}10^{-3}$
Linear Drag Coefficient (Ns/m)	c_d^l	$-6.5{\cdot}10^{-4}$
Rotational Drag Coefficient (Nms/rad)	c_d^r	$-2.2{\cdot}10^{-6}$
Catheter Coil Dipole Moment (Am^2)	$\|\boldsymbol{\mu}_c\|$	0.09

We assume that the state of the capsule evolves in time subject to magnetic wrench $(\mathbf{w}_\mu^p)$, (buoyancy-adjusted) gravitational force $(\mathbf{F}_g^p \in \mathbb{R}^3)$ and drag force $(\mathbf{F}_d^p \in \mathbb{R}^3)$ and torque $(\boldsymbol{\tau}_d^p \in \mathbb{R}^3)$. Using (1) extended by a quaternion-based magnetic torque model from [4], we represent the dynamics of the capsule as follows:

$$ {}^{\mathcal{G}}_{\mathcal{P}}\dot{\mathbf{p}} = {}^{\mathcal{G}}_{\mathcal{P}}\mathbf{v}, \tag{17} $$

$$ {}^{\mathcal{G}}_{\mathcal{P}}\dot{\mathbf{v}} = \frac{1}{m_p}\left(\|\boldsymbol{\mu}_p\| \nabla \mathbf{B}_p {}^{\mathcal{G}}_{\mathcal{P}}\hat{\mathbf{z}} - \mathbf{F}_d^p({}^{\mathcal{G}}_{\mathcal{P}}\mathbf{v}) - \mathbf{F}_g^p\right), \tag{18} $$

$$ {}^{\mathcal{G}}_{\mathcal{P}}\dot{\mathbf{o}} = \frac{1}{2}\begin{bmatrix} -\mathbf{o}_v^T \\ \mathbf{o}_c\mathbf{I}_3 - S(\mathbf{o}_v) \end{bmatrix} {}^{\mathcal{P}}_{\mathcal{P}}\boldsymbol{\omega}, \tag{19} $$

$$ {}^{\mathcal{P}}_{\mathcal{P}}\dot{\boldsymbol{\omega}} = \mathbf{M}^{-1}\left(\|\boldsymbol{\mu}_p\| S\left(\begin{bmatrix} 0 & 0 & 1 \end{bmatrix}^T\right) {}^{\mathcal{G}}_{\mathcal{P}}\mathbf{R}\,\mathbf{B}_p + \boldsymbol{\tau}_d^p\right) \tag{20} $$

where $m_p \in \mathbb{R}^+$ is the mass of the capsule and $\mathbf{M} \in \mathbb{R}^{3\times3}$ is its inertia matrix expressed in frame $(\{\mathcal{P}\})$. Note that the frame $(\{\mathcal{P}\})$ is fitted such that the direction of the magnetic dipole moment coincides with its Z-axis.

B. Model Identification and Validation

The identification of the parameters of the capsule model (17)–(20) comprises a series of characterization tests. The results of these tests are presented in Table I. The mass (m_p) of the capsule is measured using precision scales (Mettler Toledo, Greifensee, Switzerland). By approximating the volume of the capsule as a cylinder, we can subsequently use this metric to estimate the inertia matrix $(\mathbf{M})$ and buoyancy-adjusted gravity force $(\mathbf{F}_g^p)$.

In this study, we neglect the cross-dependence between rotational and translational motion of the capsule, and assume no turbulences to occur in the fluid environment. Hence, we use the linear viscous drag model. We assume the drag force $(\mathbf{F}_d^p)$ and torque $(\boldsymbol{\tau}_d^p)$ to be linearly dependent on the translational and rotational velocities as follows:

$$ \mathbf{F}_d^p = c_d^l {}^{\mathcal{G}}_{\mathcal{P}}\mathbf{v} \tag{21} $$

$$ \boldsymbol{\tau}_d^p = c_d^r \mathbf{I}_{3\times3} {}^{\mathcal{P}}_{\mathcal{P}}\boldsymbol{\omega} \tag{22} $$

where $c_d^l \in \mathbf{R}^-$ and $c_d^r \in \mathbf{R}^-$ are the viscous linear and rotational drag coefficients. We identify these coefficients along with the magnetic dipole moment $\boldsymbol{\mu}_p$ in a characterization experiment, whereby an optical camera (BlackflyS, FLIR Systems, Wilsonville, OR, USA) is used to record the motion of the capsule actuated by the ARMM system in an enclosed channel. The pose of the capsule is segmented manually and the coefficients are fitted using linear regression.

The model is validated experimentally (Fig. 9). We use two BlackflyS cameras to record five independent projectile ejections for each of four different configurations of the control system. A measurement grid is placed at the distal end of the workspace. The location of this collision is manually segmented from the camera images.

Subsequently, each ejection is simulated using the identified state-space model. The predicted collision location is compared with the experimental data. We record a mean estimation error of 6.48 mm for all trials. The capsule motion is considered repeatable, with the spread between observed collision locations quantified with a standard deviation of 3.82 mm. Additionally, we use the simulations to provide a quantitative estimate of projectile velocities. Across all ejections, the mean initial velocity norm is 0.054 m/s, the mean impact velocity is 1.9 m/s, and the average velocity is 0.67 m/s.

VI. PROJECTILE DELIVERY

The model (17)–(20) allows us to predict the projectile trajectory $(\boldsymbol{\pi}(t;\, {}^{\mathcal{G}}_{\mathcal{C}}\mathbf{H}, \boldsymbol{\sigma} : \mathbb{R}_{\geq 0} \mapsto \mathrm{SE}(3)))$. This trajectory is dependent on a given catheter tip pose $({}^{\mathcal{G}}_{\mathcal{C}}\mathbf{H})$ and the configuration $(\boldsymbol{\sigma})$ of the position control system (Fig. 7). By influencing these parameters, the capsule trajectory can be changed, directing it toward a specified final destination. In this section, we introduce one such technique, reconfiguring the ARMM system within the null-space of magnetic actuation. This allows us to guide the projectile toward a specific target while keeping the catheter tip steady.

A. Null-Space Targeting Approach

The most complete way of stabilizing the catheter tip during the targeting involves reconfiguration within the null-space of the overactuated position control system (14) The kernel $(\ker(\mathbf{A}) \in \mathbb{R}^{5\times2})$ of that system offers two degrees of freedom for system reconfiguration. In practice, realizing the targeting this way is challenging. Inherently, the matrix $\mathbf{A}$ is badly scaled, as it links the tip velocity to control variables (positions, rotations, and current) with different characteristics and limits. This leads to a variety of problems, whereby the system limits are exhausted during operation (e.g., the mobile coil collides with the workspace) The weighted least-squares approach, used to handle these, cannot be translated directly into the null-space motion.

Therefore, we propose an alternative solution (Fig. 10). For a given configuration of the catheter, we perform the targeting by using the null-space of the magnetic wrench acting on its tip. In principle, by keeping the wrench constant, the catheter should experience no motion throughout the targeting.

We make our strategy feasible by introducing additional assumptions. We do not reconfigure the system along the radius (r) of the spherical motion to reduce the likelihood of the collision of the mobile electromagnet with the workspace. Additionally, we assume that this fixed radius is large enough such that the magnetic force $(\mathbf{f}_\mu)$ does not play a significant role in the

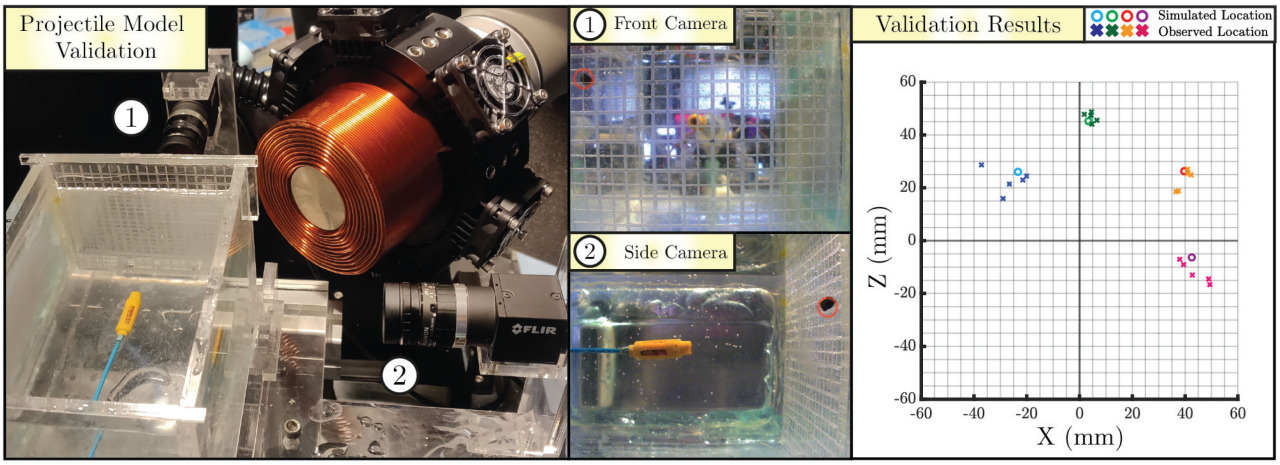

Fig. 9. We validate the projectile model by ejecting the capsule toward a transparent measurement grid. In total, five ejections are performed at each of the four different system configurations. Each ejection is recorded by two USB3 cameras ① and ② (BlackflyS, FLIR Systems, Wilsonville, OR, USA) at 90 frames per second. The recordings are segmented to measure the collision points of the capsule (red circles) with the measurement grid. Subsequently, the identified state-space model (17)–(20) is used to simulate the ejection followed by the collision with the grid in corresponding system configurations. The simulated and observed collision locations are compared to assess the accuracy and precision of the delivery. (Please refer to the video supplementary material for the demonstration of this experiment.)

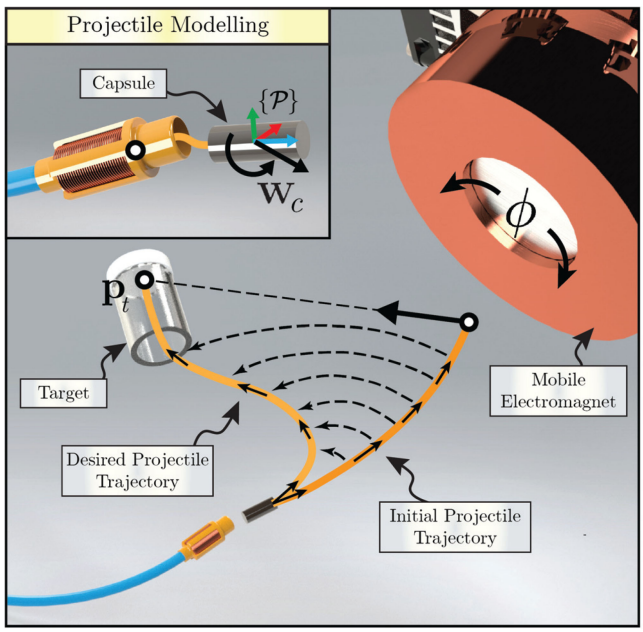

Fig. 10. We guide the capsule ejected from the catheter to a target located at the position ($\mathbf{p}_t \in \mathbb{R}^3$) using an open-loop strategy. Upon ejection, the capsule moves as a projectile due to a net wrench ($\mathbf{w}_c \in \mathbb{R}^6$) comprising the gravity, drag, and magnetic force/torque. Our strategy seeks to influence that motion by changing the configuration of the catheter control system before capsule ejection. We reconfigure the angle ($\phi \in \mathbb{S}$) of the spherical motion and the current ($I \in \mathbb{R}$) inside the mobile electromagnet to modify the predicted trajectory of the capsule such that it reaches the target.

actuation [5], [7], [24]. This assumption has been verified by analyzing the experimental data from Fig. 8 in terms of magnetic force contribution to catheter deflection. Specifically, the mean contribution of force to the bending moment at the catheter base was, on average, the 6.12% of the total moment across all collected samples.

The resulting reduced null-space spans a single vector defined by the kernel of reduced spherical actuation as follows:

$$\widehat{\boldsymbol{\nu}} = \ker\left(\begin{bmatrix} \frac{\partial \boldsymbol{\tau}_\mu}{\partial \theta} & \frac{\partial \boldsymbol{\tau}_\mu}{\partial \phi} & \frac{\partial \boldsymbol{\tau}_\mu}{\partial I} \end{bmatrix}\right) \in \mathbb{R}^{3\times 1} \tag{23}$$

where ker() is the matrix kernel computed using singular value decomposition. The reconfiguration in the direction described by this kernel should cause negligible motion of the catheter tip, allowing us to modify the expected capsule trajectory.

B. *Targeting Simulations and Experiments*

We illustrate the capabilities of our targeting approach in a few studies. First of all, we want to evaluate the range of possible targets offered by our approach. For that purpose, we use four representative system configurations taken from catheter control experiments (Fig. 8). For each configuration, we simulate the maximum range of motions within null-space (23), permitted by the physical limits of our system. Using the capsule model (17)–(20), we compute trajectories associated with a number of configurations within each motion range (Fig. 11). We observe that the null-space reconfiguration effectively involves only the current (I) and the angle (ϕ). This fact can be explained by inspection, noting that in (9), both components of magnetic torque depend on the same product of these two variables, which cannot counterbalance any change to (θ). Additionally, we observe strong dependence on the range of possible trajectories on the initial value of the current for a given configuration. The configurations with larger initial currents offer more limited targeting possibilities.

Subsequently, we perform a targeting trial (Fig. 12). The ARMM system is reconfigured within the null-space of magnetic actuation. The motion is programmed such that the angle (ϕ) increases steadily. For each iteration, the predicted trajectory corresponding to a given system configuration is calculated. If the distance between the location of the target and the prediction

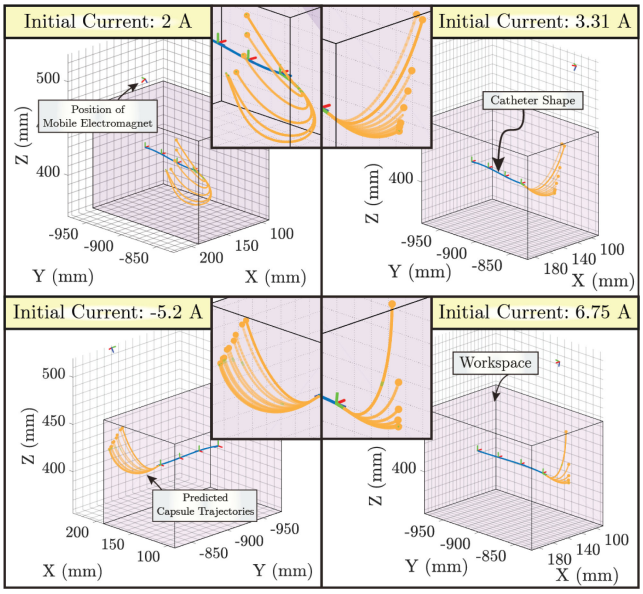

Fig. 11. For any given configuration of the magnetically actuated catheter (blue), a range of trajectories (orange) achievable using the null-space reconfiguration can be estimated using our dynamic model. We demonstrate such estimates for four representative snapshots from the catheter control experiment (Fig. 8). For each trajectory, the null-space reconfiguration has been simulated between the physical bounds of the system. For each simulated configuration, we used the dynamic model to calculate the associated predicted trajectory.

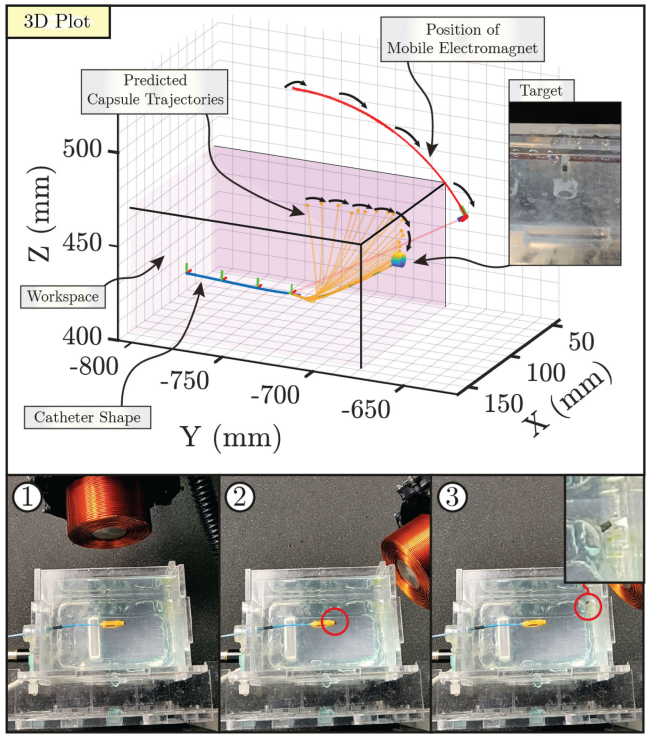

Fig. 12. Trajectory prediction is used to deliver the projectile to a target within the workspace. ① The mobile electromagnet is aligned with the catheter. The catheter is deflected to the ejection position. ② The targeting algorithm is used to change the configuration of the mobile electromagnet along the null-space of magnetic actuation. During the reconfiguration, the dynamic model of the capsule is used online to predict the capsule trajectory. We perform consecutive ultrasound scans to estimate the residual displacement of the catheter. The mean displacement during the trial is 0.80 mm. Once any point along the trajectory is sufficiently close (below 1 mm) to the target, the reconfiguration stops. ③ The mobile electromagnet is activated and the projectile is ejected from the catheter toward the target. (Please refer to the video supplementary material for the demonstration of this experiment.)

is less than 1 mm, the reconfiguration stops and the capsule ejection takes place. The mean residual catheter tip displacement during the reconfiguration is 0.80 mm.

Finally, we demonstrate the successful delivery and retrieval of a projectile, ejecting it to a target beyond the reach of catheter tip (Fig. 13). We use our targeting approach to find a suitable configuration of the ARMM system. We record two representative trials using a MotionBlitz *EoSens* Cube7 high-speed camera (Mikrotron GmbH, Unterschleißheim, Germany) at 1000 FPS. In the first trial, the capsule reaches the cylindrical hole within the target. In the second trial, the capsule hits the main body of the target and comes to rest on it due to the magnetic actuation still active (as in Fig. 2). Upon switching off the magnetic actuation, the capsule falls off from the target and is successfully retrieved by the magnetic field of the miniaturized electromagnet.

VII. Discussion

The experimental work presented in this article demonstrates that a magnetic catheter can successfully be used as a delivery vehicle for untethered agents. By using external magnetic fields provided by a mobile electromagnet, the catheter can be steered into the vicinity of the target. Subsequently, the catheter can eject the capsule which is delivered to the target as a projectile. Overactuation of the system can be used to determine the final trajectory of the projectile, effectively allowing us to aim at a selected target.

The principal factor, which restricts the performance of our system at all stages of the delivery procedure, is a slow tracking rate of the scanning ultrasound. As we rely only on this modality for state feedback, the effective rate of our controllers is approximately 0.14 Hz. This results in mean control errors of above 1.25 mm, which are effectively higher than the ones (below 1 mm) reported in comparable previous work involving high-speed optical tracking (which is nevertheless not a clinically relevant tracking modality) [4], [6]. Furthermore, such a low control rate has a negative impact on the stability of the system. This predominantly affects the ability of the inner control loop to enforce spherical motion at larger deflections of the catheter, where significant magnetic forces are present. However, despite these limitations, scanning ultrasound can be considered a feasible option for real-time tracking in these situations, where information on the full shape of the catheter is required. It remains particularly relevant for magnetically actuated devices, which prohibit the use of high-resolution, high-bandwidth modalities, such as electromagnetic trackers.

There are several ways in which the shape reconstruction rate of the ultrasound could be improved. The use of fluoroscopy can be considered a viable, albeit less safe alternative [25]. Safer methods could involve using three-dimensional ultrasound transducers or combining the ultrasound with Fiber-Bragg Grating (FBG) based proprioceptive shape sensing [26]–[28]. Finally, multirate state observers could be used to combine

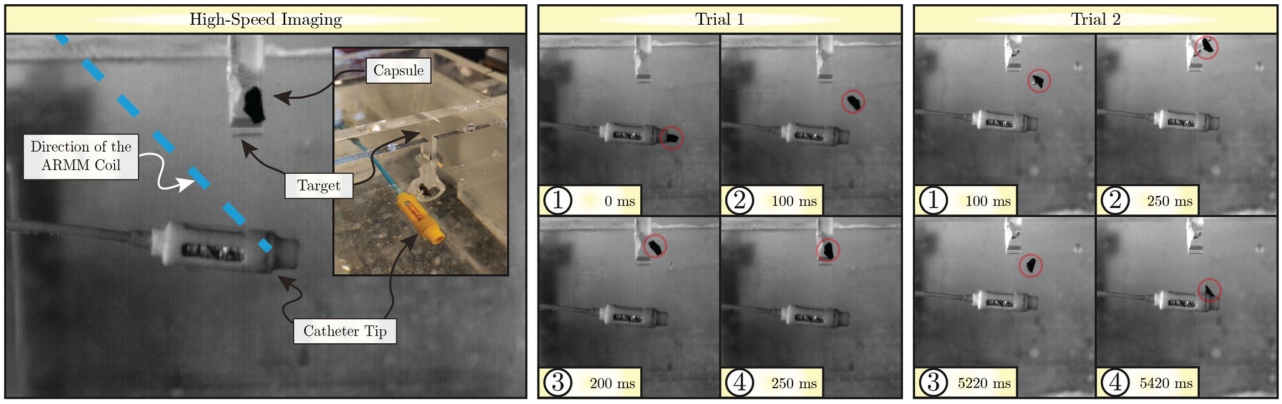

Fig. 13. We demonstrate the advantage of our approach, by using the capsule to reach a target unattainable by the catheter tip. We use a MotionBlitz *EoSens* Cube7 high-speed camera (Mikrotron GmbH, Unterschleißheim, Germany) to register the capsule motion ① – ④) upon ejection from the catheter in two trials. We image the workspace at 1000 FPS. In the first trial, the capsule is guided toward a cylindrical opening in the target, where it remains after the magnetic field has been turned off. In the second trial, the capsule reaches the target and remains attached to it for 5 s. After 5 s, the external magnetic field is switched off. The capsule falls off the target toward the catheter tip. Once close to the catheter, it is successfully retrieved by a miniaturized electromagnet. (Please refer to the video supplementary material for the demonstration of this experiment.)

estimation-based methods and the scanning ultrasound for improved effective feedback rate [29].

Another aspect, where improvements can be made regarding the catheter control, involves replacing the spherical motion actuation model with a more complex framework. The spherical motion is burdened with inherent singularities, which occur when the coil current (I) is zero and when (ϕ) reaches 90°. Throughout the experiments, we observed that, by the use of damping in our inverse model, the current singularity poses no problem to the performance of the system, as demonstrated in Trajectory 1 (Fig. 8). Nevertheless, replacing the spherical motion control with another approach, capable of obstacle avoidance, could alleviate this problem. Additionally, this would allow us to disregard the bandwidth of the feedback as a factor limiting the catheter stability at larger deflections. Additionally, such state observers could potentially be used to reduce the noise within the system. This is particularly important for the long-axis noise within the shape sensing method, which was first reported in [6] and observed again to degrade the catheter control performance within the experiments in this work.

Regarding the projectile delivery, our work demonstrates the potential of magnetic capsules as viable tools extending the reach of the catheter into the places inaccessible to its tip. We show that such capsules can be effectively targeted in open loop using the null-space of catheter actuation. With the reported targeting accuracy of 6.48 mm, we consider them sufficiently precise for clinically relevant tasks, such as targeted drug delivery or biopsies.

The experiments presented in this work do not exhaust the subject of magnetic projectiles. The characterization of complete trajectories (both in terms of the capsule positions and velocities) and their comparison with the ones predicted by our model is required as a complete experimental proof of our modeling approach. Additionally, further studies are required to establish the accuracy of capsule targeting in biological fluids or in the presence of fluid flow.

In our work, we utilize a single mobile electromagnet as a source of external field. This significantly limits the range of trajectories, which can be achieved with a capsule launched from a catheter with particular configuration. One possible solution could involve modification of the targeting approach. Instead of remaining stationary, the catheter tip may be actively guided to a configuration, in which the capsule can be ejected on a trajectory reaching the desired target. Additionally, the magnetic actuation system could be expanded to involve several independent mobile coils. This should vastly enhance both the targeting capabilities of our system as well as the set of reachable targets [24]. Nevertheless, such actuation systems would potentially require a different targeting strategy due to more complex magnetic field patterns they generate.

An important aspect of our concept that has not been exhaustively addressed in this work is the retrieval of the capsules back to the catheter. Thus far, we show that by bringing the capsule into the vicinity of the catheter tip, it gets attracted to the outer shell of the dock. It remains unclear whether such a retrieval would allow for safe retraction of the catheter in a clinically relevant scenario. Tethering the capsule in a manner similar to [18] could potentially alleviate this issue by allowing for retrieval directly into the dock. Nevertheless, the presence of a tether would alter the dynamic behavior of the capsule, rendering our state-space trajectory model invalid. Alternative solutions could involve biodegradation of the capsule, which nevertheless remains problematic due to the inflammatory nature of magnetic materials [30].

VIII. Conclusion

In this article, we presented a magnetic catheter capable for controller release and retrieval of untethered magnetic capsules. We used the mobile electromagnet of the ARMM system as a source of external field for magnetic actuation. In our study, the catheter was steered into the vicinity of the target with a closed-loop position controller under the guidance of scanning ultrasound. The capsule was ejected from the catheter by reversing the polarity of the miniaturized electromagnet attached

to its tip. The released capsule moves as a projectile. We used a dynamic model of the capsule to predict the trajectory of the projectile. We demonstrated that the trajectory of the capsule can be controlled by reconfiguring the ARMM system within the null-space of the magnetic actuation.

Our catheter was tested in a series of experiments. We first determined the accuracy of the catheter shape reconstruction using scanning ultrasound, reporting the lowest mean error of 0.37 mm. Subsequently, we use our closed-loop controller to guide the catheter along a set of trajectories with the lowest mean error of 0.82 mm. We validated the accuracy of the capsule model, reporting a mean target estimation error of 6.48 mm and an average spread of 3.82 mm between launches at the same target. Finally, we realized projectile delivery experiments, demonstrating successful targeting with a mean catheter tip displacement of 0.80 mm, and a delivery and retrieval from a challenging location.

In future work, we will improve the control bandwidth of our catheter, by incorporating faster shape reconstruction modalities such as FBG sensors and 3-D ultrasound. We will also expand our control technique to enable the use of mobile electromagnet at any orientation with respect to the catheter tip. We will enhance our dynamical model, improving the drag modeling and enabling the simulations predicting the success of projectile retrieval. This way, we will create a comprehensive and accurate planning framework for capsule delivery to a given target, also in clinically relevant conditions involving biological motion, such as blood flow. Finally, we hope to use the principles presented in this article to create advanced, clinically relevant functionalized catheters. The aspects we will put a particular emphasis on will involve miniaturization of our capsules and independent delivery of multiple projectiles within a single insertion. We envision that future prototypes of such catheters will be capable of engaging the human body by utilizing a large variety of functional microscale modules integrated into their structure. Such catheters will form part of versatile platforms capable of accomplishing advanced (micro-)surgical tasks and improving patient care.

APPENDIX

The spherical actuation Jacobian $(\mathbf{J}_s)$ is defined as follows:

$$(\mathbf{J}_s) = \begin{bmatrix} \frac{\partial \mathbf{w}}{\partial r} & \frac{\partial \mathbf{w}}{\partial \theta} & \frac{\partial \mathbf{w}}{\partial \phi} & \frac{\partial \mathbf{w}}{\partial I} \end{bmatrix} \tag{24}$$

and is derived from model (9). The field $(b(r, I))$ and gradient maps within that model were presented in our previous work [19]. They have the nonlinear form

$$b(r, I) = \left(b_w(r) + \eta(I) b_c(r)\right), \tag{25}$$

$$\frac{\partial b}{\partial r} = \left(\frac{\partial b_w}{\partial r} + \eta(I)\frac{\partial b_c}{\partial r}\right) \tag{26}$$

where $b_w(r)$, $b_c(r) : \mathbb{R}^+ \mapsto \mathbb{R}^+$ are unit field maps for the windings and the core of the mobile electromagnet, respectively. The coefficient $(\eta(I) \in (0, 1])$ is used to take into account the saturation of electromagnet core, which happens above $\pm$ 15 A. Combining (9) with (25) and (26), we can analytically derive the individual columns of (24) as follows:

$$\frac{\partial \mathbf{w}}{\partial r} = I\mu \begin{bmatrix} -1.5\ \sin\theta\ \sin\phi\ \cos\phi \frac{\partial^2 b}{\partial r^2} \\ 1.5\ \cos\theta\ \sin\phi\ \cos\phi \frac{\partial^2 b}{\partial r^2} \\ (\sin^2\phi - 0.5\ \cos^2\phi) \frac{\partial^2 b}{\partial r^2} \\ -\cos\theta\ \cos\phi \frac{\partial b}{\partial r} \\ -\sin\theta\ \cos\phi \frac{\partial b}{\partial r} \\ 0 \end{bmatrix} \tag{27}$$

$$\frac{\partial \mathbf{w}}{\partial \theta} = I\mu \begin{bmatrix} -1.5\ \cos\theta\ \sin\phi\ \cos\phi \frac{\partial b}{\partial r} \\ -1.5\ \sin\theta\ \sin\phi\ \cos\phi \frac{\partial b}{\partial r} \\ 0 \\ \sin\theta\ \cos\phi\ b(r, I) \\ -\cos\theta\ \cos\phi\ b(r, I) \\ 0 \end{bmatrix} \tag{28}$$

$$\frac{\partial \mathbf{w}}{\partial \phi} = I\mu \begin{bmatrix} 1.5\ \sin\theta \left(\cos^2\phi - \sin^2\phi\right) \frac{\partial b}{\partial r} \\ 1.5\ \cos\theta \left(\cos^2\phi - \sin^2\phi\right) \frac{\partial b}{\partial r} \\ 3\ \sin\phi\ \cos\phi\ \frac{\partial b}{\partial r} \\ \cos\theta\ \sin\phi\ b(r, I) \\ \sin\theta\ \sin\phi\ b(r, I) \\ 0 \end{bmatrix} \tag{29}$$

$$\frac{\partial \mathbf{w}}{\partial I} = \mu \begin{bmatrix} -1.5\ \sin\theta\ \sin\phi\ \cos\phi \left(\frac{\partial b}{\partial r} + I\ \frac{\partial b_c}{\partial r} \frac{\partial \eta}{\partial I}\right) \\ 1.5\ \cos\theta\ \sin\phi\ \cos\phi \left(\frac{\partial b}{\partial r} + I\ \frac{\partial b_c}{\partial r} \frac{\partial \eta}{\partial I}\right) \\ (\sin^2\phi - 0.5\ \cos^2\phi) \left(\frac{\partial b}{\partial r} + I\ \frac{\partial b_c}{\partial r} \frac{\partial \eta}{\partial I}\right) \\ -\cos\theta\ \cos\phi \left(b(r, I) + I\ b_c \frac{\partial \eta}{\partial I}\right) \\ -\sin\theta\ \cos\phi \left(b(r, I) + I\ b_c \frac{\partial \eta}{\partial I}\right) \\ 0 \end{bmatrix}. \tag{30}$$

REFERENCES

[1] J. J. Abbott, E. Diller, and A. J. Petruska, "Magnetic methods in robotics," *Annu. Rev. Control, Robot., Auton. Syst.*, vol. 3, pp. 57–90, 2020.

[2] A. Ali, D. H. Plettenburg, and P. Breedveld, "Steerable catheters in cardiology: Classifying steerability and assessing future challenges," *IEEE Trans. Biomed. Eng.*, vol. 63, no. 4, pp. 679–693, Apr. 2016.

[3] T. Greigarn, N. L. Poirot, X. Xu, and M. C. Çavuşoğlu, "Jacobian-based task-space motion planning for MRI-actuated continuum robots," *IEEE Robot. Autom. Lett.*, vol. 4, no. 1, pp. 145–152, Jan. 2019.

[4] J. Edelmann, A. J. Petruska, and B. J. Nelson, "Magnetic control of continuum devices," *Int. J. Robot. Res.*, vol. 36, no. 1, pp. 68–85, 2017.

[5] F. Ullrich, S. Schuerle, R. Pieters, A. Dishy, S. Michels, and B. J. Nelson, "Automated capsulorhexis based on a hybrid magnetic-mechanical actuation system," in *Proc. IEEE Int. Conf. Robot. Autom.*, 2014, pp. 4387–4392.

[6] J. Sikorski, A. Denasi, G. Bucchi, S. Scheggi, and S. Misra, "Vision-based 3-D control of magnetically actuated catheter using BigMag-an array of mobile electromagnetic coils," *IEEE/ASME Trans. Mechatronics*, vol. 24, no. 2, pp. 505–516, Apr. 2019.

[7] C. Chautems, A. Tonazzini, D. Floreano, and B. J. Nelson, "A variable stiffness catheter controlled with an external magnetic field," in *Proc. IEEE/RSJ Int. Conf. Intell. Robots Syst.*, 2017, pp. 181–186.

[8] J. Sikorski, E. S. Rutting, and S. Misra, "Grasping using magnetically-actuated tentacle catheter: A proof-of-concept study," in *Proc. 7th IEEE Int. Conf. Biomed. Robot. Biomechatronics*, 2018, pp. 609–614.

[9] S. L. Charreyron, E. Gabbi, Q. Boehler, M. Becker, and B. J. Nelson, "A magnetically steered endolaser probe for automated panretinal photocoagulation," *IEEE Robot. Autom. Lett.*, vol. 4, no. 2, pp. 284–290, Apr. 2019.

[10] B. J. Nelson, I. K. Kaliakatsos, and J. J. Abbott, "Microrobots for minimally invasive medicine," *Annu. Rev. Biomed. Eng.*, vol. 12, pp. 55–85, 2010.

[11] X. Chen *et al.*, "Small-scale machines driven by external power sources," *Adv. Mater.*, vol. 30, no. 15, 2018, Art. no. 1705061.
[12] A. Vikram Singh and M. Sitti, "Targeted drug delivery and imaging using mobile milli/microrobots: A promising future towards theranostic pharmaceutical design," *Curr. Pharmaceut. Des.*, vol. 22, no. 11, pp. 1418–1428, 2016.
[13] Q. Jin, Y. Yang, J. A. Jackson, C. Yoon, and D. H. Gracias, "Untethered single cell grippers for active biopsy," *Nano Lett.*, vol. 20, no. 7, pp. 5383–5390, 2020.
[14] J. Leclerc, A. Ramakrishnan, N. V. Tsekos, and A. T. Becker, "Magnetic hammer actuation for tissue penetration using a millirobot," *IEEE Robot. Autom. Lett.*, vol. 3, no. 1, pp. 403–410, Jan. 2018.
[15] M. Sitti *et al.*, "Biomedical applications of untethered mobile milli/microrobots," *Proc. IEEE*, vol. 103, no. 2, pp. 205–224, Feb. 2015.
[16] J. Burgner-Kahrs, D. C. Rucker, and H. Choset, "Continuum robots for medical applications: A survey," *IEEE Trans. Robot.*, vol. 31, no. 6, pp. 1261–1280, Dec. 2015.
[17] A. Ali *et al.*, "Catheter steering in interventional cardiology: Mechanical analysis and novel solution," *Proc. Inst. Mech. Eng. Part H: J. Eng. Med.*, vol. 233, no. 12, pp. 1207–1218, 2019.
[18] C. Chautems and B. J. Nelson, "The tethered magnet: Force and 5-DOF pose control for cardiac ablation," in *Proc. IEEE Int. Conf. Robot. Autom.*, 2017, pp. 4837–4842.
[19] J. Sikorski, C. M. Heunis, F. Franco, and S. Misra, "The ARMM system: An optimized mobile electromagnetic coil for non-linear actuation of flexible surgical instruments," *IEEE Trans. Magn.*, vol. 55, no. 9, pp. 1–9, Sep. 2019.
[20] M. Kaya *et al.*, "A multi-rate state observer for visual tracking of magnetic micro-agents using 2D slow medical imaging modalities," in *Proc. IEEE/RSJ Int. Conf. Intell. Robots Syst.*, 2018, pp. 1–8.
[21] R. M. Murray, Z. Li, and S. S. Sastry, *A Mathematical Introduction to Robotic Manipulation*, vol. 29, Boca Raton: CRC Press, 1994.
[22] A. J. Petruska, J. Edelmann, and B. J. Nelson, "Model-based calibration for magnetic manipulation," *IEEE Trans. Magn.*, vol. 53, no. 7, pp. 1–6, Jul. 2017.
[23] A. S. Deo and I. D. Walker, "Overview of damped least-squares methods for inverse kinematics of robot manipulators," *J. Intell. Robotic Syst.*, vol. 14, no. 1, pp. 43–68, 1995.
[24] X. Du, M. Zhang, J. Yu, L. Yang, W. Y. P. Chiu, and L. Zhang, "Design and real-time optimization for a magnetic actuation system with enhanced flexibility," *IEEE/ASME Trans. Mechatronics*, vol. 26, no. 3, pp. 1524–1535, Jun. 2021.
[25] A. Hong, A. J. Petruska, and B. J. Nelson, "Tracking a magnetically guided catheter with a single rotating c-arm," in *Proc. IEEE Int. Conf. Robot. Autom.*, 2015, pp. 618–623.
[26] C. Nadeau, H. Ren, A. Krupa, and P. E. Dupont, "Intensity-based visual servoing for instrument and tissue tracking in 3D ultrasound volumes," *IEEE Trans. Autom. Sci. Eng.*, vol. 12, no. 1, pp. 367–371, Jan. 2015.
[27] P. Chatelain, A. Krupa, and N. Navab, "3D ultrasound-guided robotic steering of a flexible needle via visual servoing," in *Proc. IEEE Int. Conf. Robot. Autom.*, 2015, pp. 2250–2255.
[28] A. Denasi *et al.*, "An observer-based fusion method using multicore optical shape sensors and ultrasound images for magnetically-actuated catheters," in *Proc. IEEE Int. Conf. Robot. Autom.*, 2018, pp. 50–57.
[29] J. Edelmann, A. J. Petruska, and B. J. Nelson, "Estimation-based control of a magnetic endoscope without device localization," *J. Med. Robot. Res.*, vol. 3, no. 1, 2018, Art. no. 1850002.
[30] K. T. Nguyen *et al.*, "A magnetically guided self-rolled microrobot for targeted drug delivery, real-time x-ray imaging, and microrobot retrieval," *Adv. Healthcare Mater.*, vol. 10, no. 6, 2021, Art. no. 2001681.

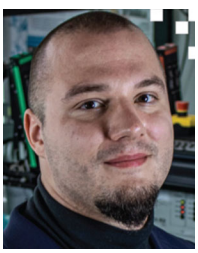

Jakub Sikorski (Member, IEEE) received the M.Eng. degree in biomedical engineering from the University of Glasgow, Glasgow, U.K., in 2015 and the Ph.D. degree in biomechanical engineering from the University of Twente, Enschede, The Netherlands, in 2020.

He is currently a Postdoctoral Researcher with the Surgical Robotics Laboratory, University of Twente. His research interests include continuum and soft robotics, magnetic devices, mechatronic design, and control of biomedical systems.

Christoff Marthinus Heunis (Student Member, IEEE) received the M.Sc. degree in mechatronic engineering from the University of Stellenbosch, Stellenbosch, South Africa, in 2016 and the Ph.D. degree in biomechanical engineering from the University of Twente, Enschede, The Netherlands, in 2021.

He is currently a Postdoctoral Researcher with the Surgical Robotics Laboratory, University of Twente. His research interests include the design of clinical equipment for the treatment of cardiovascular and oncological disorders.

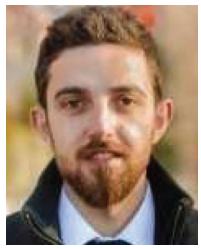

Rafic Obeid received the B.Sc. degree in biomedical engineering and the M.Sc. degree in mechatronics engineering from the Polytechnic of Turin, Turin, Italy, in 2014 and 2017, respectively.

In 2017, he joined the Surgical Robotics Laboratory, University of Twente, Enschede, The Netherlands, to work on his master's thesis on development of scanning ultrasound techniques for shape reconstruction of continuum manipulators. He is currently a Field Application Engineer with the Delta Electronics, Hoofddorp, The Netherlands.

Venkatasubramanian Kalpathy Venkiteswaran (Member, IEEE) received the Ph.D. degree in mechanical engineering from The Ohio State University, Columbus, OH, USA, in 2017.

He is currently an Assistant Professor with the Department of Biomechanical Engineering, University of Twente, Enschede, The Netherlands. Prior to that, he was a Postdoctoral Fellow with the Surgical Robotics Laboratory, University of Twente for two years. His research interests include design of soft robots and flexible devices, with a focus on medical applications.

Sarthak Misra (Senior Member, IEEE) received the master's degree from McGill University, Montreal, QC, Canada, in 2001, and the Ph.D. degree from the Johns Hopkins University, Baltimore, MD, USA, in 2009, both in mechanical engineering.

He is currently a Full Professor with the Department of Biomechanical Engineering, University of Twente, Enschede, The Netherlands, and with the Department of Biomedical Engineering, University of Groningen and University Medical Center Groningen, Groningen, The Netherlands. Prior to commencing his doctoral studies, he was a Dynamics and Controls Analyst with the International Space Station Program. His research interests include surgical robotics and medical microrobotics.

Prof. Misra was the recipient of the European Research Council Starting, Proof-of-Concept, and Consolidator Grants and the Netherlands Organization for Scientific Research VENI and VIDI Awards. He is a Co-Chair of the Robotics and Automation Society Technical Committee on Surgical Robotics and a Co-Chair of the International Federation of Automatic Control Technical Committee on Biological and Medical Systems.